INFECTION AND IMMUNITY, Sept. 2011, p. 3527–3540 Vol. 79, No. 9
0019-9567/11/$12.00 doi:10.1128/IAI.05139-11

Differential Response of the Human Renal Proximal Tubular Epithelial Cell Line HK-2 to Shiga Toxin Types 1 and 2[▽]

Erin K. Lentz, Dinorah Leyva-Illades, Moo-Seung Lee, Rama P. Cherla, and Vernon L. Tesh*

Department of Microbial and Molecular Pathogenesis, College of Medicine, Texas A&M Health Science Center, Bryan, Texas 77807

Received 28 March 2011/Returned for modification 23 April 2011/Accepted 4 June 2011

Shiga toxins (Stxs) are expressed by the enteric pathogens *Shigella dysenteriae* serotype 1 and certain serotypes of *Escherichia coli*. Stx-producing bacteria cause bloody diarrhea with the potential to progress to acute renal failure. Stxs are potent protein synthesis inhibitors and are the primary virulence factors responsible for renal damage that may follow diarrheal disease. We explored the use of the immortalized human proximal tubule epithelial cell line HK-2 as an *in vitro* model of Stx-induced renal damage. We showed that these cells express abundant membrane Gb_3 and are differentially susceptible to the cytotoxic action of Stxs, being more sensitive to Shiga toxin type 1 (Stx1) than to Stx2. At early time points (24 h), HK-2 cells were significantly more sensitive to Stxs than Vero cells; however, by 72 h, Vero cell monolayers were completely destroyed while some HK-2 cells survived toxin challenge, suggesting that a subpopulation of HK-2 cells are relatively toxin resistant. Fluorescently labeled Stx1 B subunits localized to both lysosomal and endoplasmic reticulum (ER) compartments in HK-2 cells, suggesting that differences in intracellular trafficking may play a role in susceptibility to Stx-mediated cytotoxicity. Although proinflammatory cytokines were not upregulated by toxin challenge, Stx2 selectively induced the expression of two chemokines, macrophage inflammatory protein-1α (MIP-1α) and MIP-1β. Stx1 and Stx2 differentially activated components of the ER stress response in HK-2 cells. Finally, we demonstrated significant poly(ADP-ribose) polymerase (PARP) cleavage after exposure to Stx1 or Stx2. However, procaspase 3 cleavage was undetectable, suggesting that HK-2 cells may undergo apoptosis in response to Stxs in a caspase 3-independent manner.

Shiga toxins (Stxs) are a family of genetically and functionally related cytotoxic proteins expressed by the enteric pathogens *Shigella dysenteriae* serotype 1 and certain serotypes of *Escherichia coli*. Antigenic similarity to Shiga toxin expressed by *S. dysenteriae* serotype 1 was used to define Shiga toxin type 1 (Stx1) and Stx2 expressed by Shiga toxin-producing *E. coli* (STEC) (47). Cloning and sequencing of the toxin genes revealed that Stx1 differs from the prototypical Shiga toxin by 1 amino acid, while Stx2 shares 56% sequence homology at the deduced amino acid sequence level with Shiga toxin and Stx1 (21, 46). Stxs are AB_5 toxins, consisting of a single A subunit in noncovalent association with 5 B subunits that form a pentameric ring. B subunits are responsible for binding to target cells, while the A subunit is responsible for protein synthesis inhibition (43). The toxin receptor is the neutral globo series glycolipid globotriaosylceramide (Gb_3), although one Stx2 variant toxin (Stx2e) has been shown to be capable of binding globotetraosylceramide (Gb_4) (9). Following internalization, the toxins undergo retrograde transport, which delivers the toxins to the endoplasmic reticulum (ER). A fragment of the A subunit is cleaved from the holotoxin by furin or a furin-like protease during retrograde transport. This fragment, termed the A_1 fragment, is translocated across the ER membrane using the Sec61 translocon and enters the cytosol, where it cleaves a single adenine residue from the 28S rRNA component of eukaryotic ribosomes (22, 33, 44). Stx-induced depurination leads to protein synthesis inhibition by disrupting elongation factor-dependent aminoacyl-tRNA binding to nascent polypeptides (36). Stxs have also been shown to activate host cell signaling pathways, including the ribotoxic stress response and ER stress pathways. Activation of these intracellular signaling cascades may be important for proinflammatory cytokine/chemokine production and apoptosis induction in some cell types (7, 31, 45).

Ingestion of Stx-producing bacteria may lead to the development of bloody diarrhea and, in some cases, progression to acute renal failure, termed diarrhea-associated hemolytic uremic syndrome (D^+HUS) (38). D^+HUS, a leading cause of pediatric acute renal failure, is characterized by rapid-onset oligouria or anuria, azotemia, microangiopathic hemolytic anemia with schistocytosis, and thrombocytopenia (38, 49). Histopathological examination of D^+HUS renal tissues showed that glomerular microvascular endothelial cells were frequently swollen and detached from the basement membrane and glomerular capillary lumina were occluded with fibrin-rich microthrombi (28, 40). Glomerular endothelial cells are not the only targets damaged by Stxs in the kidney. Immunohistochemical and immunofluorescence staining techniques used on murine, baboon, and human kidney sections showed that renal tubules were rich in Gb_3, and toxin overlay studies showed that Stxs bound to renal tubules (32, 51, 52). Primary human proximal tubule cells express high levels of membrane Gb_3 and are highly sensitive to Stx cytotoxicity *in vitro* (17, 26, 27). Karpman et al. (23) noted that cell damage in renal biopsy specimens from pediatric D^+HUS cases and in mice fed an Stx2-producing STEC strain was localized to the renal cortex, with pathological changes detected in both glomerular endothelial and

* Corresponding author. Mailing address: Department of Microbial and Molecular Pathogenesis, 3002 Medical Research and Education Building, Texas A&M Health Science Center, Bryan, TX 77807. Phone: (979) 436-0357. Fax: (979) 436-0360. E-mail: tesh@medicine.tamhsc.edu.

[▽] Published ahead of print on 27 June 2011.

tubular epithelial cells. Clinical studies using pediatric and geriatric renal biopsy specimens isolated from D^+HUS cases detected the presence of Stx1 and Stx2 within renal tubules (6, 54). Finally, urinary excretion of markers of proximal tubular damage, such as *N*-acetyl glucosaminidase and β_2-microglobulin, are elevated early in the course of D^+HUS, suggesting that Stx-mediated renal tubular damage may precede damage to glomerular endothelial cells (48). Collectively, these data suggest that proximal tubules may be an important early target of the toxins and that damage to renal tubules may contribute to the progression of disease leading to glomerular damage and the signs and symptoms of D^+HUS.

Cell culture of primary and immortalized cells has been helpful in understanding the role single cell types play in renal function, pathology, and regeneration. Ryan et al. (42) created an immortalized adult human proximal tubule epithelial cell line designated human kidney 2 (HK-2). This cell line, transformed using the human papillomavirus type 16 (HPV16) E6/E7 genes, maintains proximal tubule epithelial morphology. The goal of the present study was to characterize HK-2 cells as a suitable model to study Stx-mediated renal damage and the host response to Stx1 and Stx2. We show that HK-2 cells express high levels of membrane Gb_3 and are differentially susceptible to the cytotoxic action of Stx1 and Stx2. HK-2 cells traffic labeled Stx1 B subunits to both the lysosomal and ER compartments. Stx2 uniquely induced the expression of two chemokines, macrophage inflammatory protein 1α (MIP-1α/CCL3) and MIP-1β/CCL4. Stx1 and Stx2 differentially activate components of the ER stress response in HK-2 cells. Finally, Stxs appear to induce apoptosis in HK-2 cells by activating poly(ADP-ribose) polymerase (PARP) cleavage in a caspase 3-independent manner.

MATERIALS AND METHODS

Cell culture. The HK-2 cell line and Vero cells, an African green monkey renal epithelial cell line, were purchased from the American Type Culture Collection (Manassas, VA). HK-2 cells were maintained in complete medium consisting of keratinocyte–serum-free medium (K-SFM) supplemented with bovine pituitary extract (BPE), human recombinant epidermal growth factor (EGF) (Invitrogen, Carlsbad, CA), penicillin (100 U/ml), and streptomycin (100 μg/ml) (Gibco-BRL, Grand Island, NY) at 37°C in 5% CO_2 in a humidified incubator. The Vero cells were maintained in Dulbecco's modified Eagle's medium (DMEM) (Gibco-BRL, Grand Island, NY) supplemented with 10% fetal bovine serum (FBS) (HyClone Laboratories, Logan, UT), penicillin (100 U/ml), and streptomycin (100 μg/ml) at 37°C in humidified 5% CO_2.

Toxins. Stx1 was prepared as previously described (51). Briefly, Stx1 was purified from cell lysates prepared from *E. coli* DH5α(pCKS112) by sequential ion exchange and chromatofocusing chromatography. The purity of toxin preparations was assessed by sodium dodecyl sulfate-polyacrylamide gel electrophoresis (SDS-PAGE) with silver staining and Western blot analysis with anti-Stx1 antibodies. Toxin preparations contained <0.1 ng of endotoxin per ml, as determined by the *Limulus* amoebocyte lysate assay (Associates of Cape Cod, Falmouth, ME). Recombinant Stx2 was obtained through the NIAID, NIH Biodefense and Emerging Infections Research Resources Repository (BEI Resources) (Manassas, VA). Purified pentameric Stx1 B subunits were a kind gift from Cheleste Thorpe, Tufts University School of Medicine, Boston, MA.

Gb_3 quantification. HK-2 cells (5.0×10^5 cells) were placed in microcentrifuge tubes in 300 μl complete medium. Stxs bind to Gb_3 at 4°C; therefore, all subsequent steps were done on ice to prevent receptor internalization. Stx1 B subunits (1.2 mg/ml) were added to the cells and incubated for 1 h with gentle shaking. The cells were then centrifuged and washed twice with cold PBS. The cells were resuspended in a 1:100 dilution of anti-Stx1 B subunit murine monoclonal antibody (13C4; Hycult Biotech Inc., Plymouth Meeting, PA) for 30 min. After incubation, the cells were centrifuged and washed twice with PBS. Finally, the cells were resuspended in a 1:50 dilution of fluorescein-conjugated horse anti-mouse IgG antibody (Vector Laboratories Inc., Burlingame, CA) for 30 min. The cells were washed in PBS and analyzed by flow cytometry (FACSAria; BD Bioscience, San Jose, CA). Fluorescence parameters were gated using stained and unstained untreated cells. At least 10^4 events were measured for each sample.

Cytotoxicity assay. Vero or HK-2 cells (5.0×10^4 cells per well) were plated in 96-well plates and grown to 80% confluence at 37°C. The cells were exposed to various concentrations of Stx1 or Stx2, ranging from 100 fg/ml to 1.0 mg/ml. After incubation at 37°C in 5% CO_2 for 24, 48, or 72 h, 25 μl of 3-(4,5-dimethylthiazol-2-yl)-2,5-diphenyltetrazolium bromide (MTT) solution (5.0 mg/ml) was added to each well and incubated for 2 h at 37°C in a 5% CO_2 humidified incubator. After incubation, the plates were centrifuged for 5 min. The supernatants were removed, and 100 μl of lysis buffer (20% SDS, 50% 2-2-dimethylformamide [pH 4.7]) was added to each well. The plates were incubated at 37°C for 3 h. Optical densities (OD) were measured in an automated plate reader (Dynatech MR5000; Molecular Dynamics, Chantilly, VA). The percent cell survival was calculated as follows: [(average OD_{570} {OD at 570 nm} of treated cells − average OD_{570} of untreated control cells)/average OD_{570} of untreated control cells] × 100. Statistical significance was assessed using a *t* test in Graphpad Prism version 5 (Graphpad Software, La Jolla, CA).

Intracellular toxin trafficking. Intracellular trafficking of Stxs into HK-2 cells was determined using purified Stx1 B subunits conjugated to a fluorescent tag (Stx1 B-Alexa 488). Fifty micrograms of purified Stx1 B subunits was labeled using Alexa Fluor-488 Microscale Kits (Molecular Probes Inc., Invitrogen, Eugene, OR) as described in the manufacturer's protocol. Briefly, HK-2 cells (1.0×10^5 cells/well) were seeded overnight in four-well Lab-Tek chambered borosilicate cover glass slides (Nalge-Nunc International, Rochester, NY). The cells were washed two times with complete medium before further staining for 30 min at 37°C with cell-permeable-lysosome- or endoplasmic-reticulum-specific dye (100 nM Lyso-Tracker or 60 nM ER-Tracker live-cell staining dye; Molecular Probes Inc., Invitrogen, Eugene, OR). Complete medium containing 100 ng/ml Stx1 B-Alexa 488 was added to the cell monolayers. The cells were washed extensively and then imaged over the next 5 to 90 min. Single confocal optical sections through the middle of the majority of cells in the field of view were taken simultaneously for the red, blue, and green emission channels using a Stallion Digital Imaging Station (Carl Zeiss Microscopes, Gottingen, Germany) and SlideBook 4.2 image software (Olympus America Inc., Center Valley, PA). The images are representative of two independent experiments. All data within each experiment were collected at identical settings.

Real-time reverse transcription (RT)-PCR. HK-2 cells were exposed to either 75 pg/ml Stx1 or Stx2 for 15, 30, 60, 120, or 240 min. Total RNA was isolated using TRIzol Plus kits with an RNase-free DNase treatment (Invitrogen, Carlsbad, CA) according to the manufacturer's instructions. RNA was reverse transcribed to cDNA using a high-capacity cDNA reverse transcription kit (Applied Biosystems, Carlsbad, CA), and real-time PCR was performed on the resulting cDNAs using SYBR green I double-stranded DNA binding dye (Applied Biosystems, Carlsbad, CA). The following real-time primers were used: tumor necrosis factor alpha (TNF-α), F (5′-CCAGGCAGTCAGATCATCTTCTC-3′) and R (5′-AGCTGGTTATCTCTAGCTCCAC-3′); interleukin 1β (IL-1β), F (5′-TCCCCAGCCCTTTTGTTGA-3′) and R (5′-TTAGAACCAAATGTGGC CGTG-3′); IL-8, F (5′-AAGGAACCATCTCACTGTGTGTAAAC-3′) and R (5′-ATCAGGAAGGCTGCCAAGAG-3′); MIP-1α, F (5′-TTGTGATTGTTTG CTCTGAGAGTTC-3′) and R (5′-CGGTCGTCACCAGACACACT-5′); MIP-1β, F (5′-CCCTGGCCTTTCCTTTCAGT-3′) and R (5′-AGCTTCCTCGCGG TGTAAGA-3′); and glyceraldehyde-3-phosphate dehydrogenase (GAPDH), F (5′-CAACGGATTTGGTCGTATTGG-3′) and R (5′-GGCAACAATATCCAC TTTACCAGAGT-3′).

Real-time PCRs were carried out with 100 nM concentrations (each) of forward and reverse primers in a final volume of 25 μl. To control for the presence of contaminating DNA, reverse transcriptase-negative reaction mixtures were included. Nontemplate controls were run to test for DNA-contaminated primers. Real-time reactions were run and analyzed by using an ABI Prism 7500 sequence detection system (Applied Biosystems, Carlsbad, CA). Dissociation curves for PCR samples were made to guarantee amplification of the correct genes. The amount of mRNA, expressed as fold change, was determined from the change in threshold cycle (C_T) values normalized for GAPDH expression and then normalized to the value derived from cells at time zero prior to medium change or treatment. Statistical analyses of real-time PCR data were performed using ΔC_T values. Statistical significance was assessed at a P value of <0.05 by one-way analysis of variance (ANOVA) with Dunnett's posttest using Graphpad Prism version 5 (Graphpad Software, La Jolla, CA).

Measurement of cytokine and chemokine production. HK-2 cells were treated with 75 pg/ml Stx1 or Stx2 for 15, 30, 60, 120, or 240 min. The cellular superna-

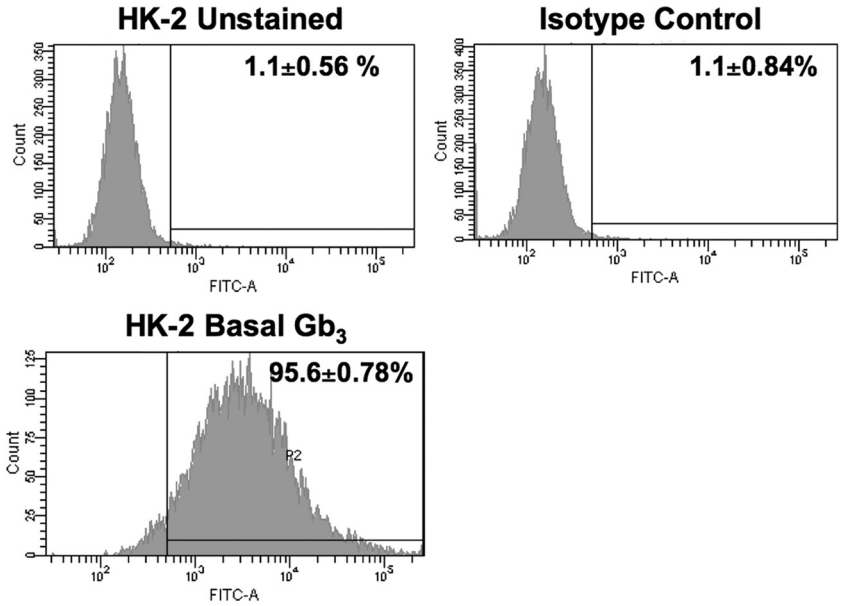

FIG. 1. Analysis of Gb_3 expression on the surfaces of HK-2 cells. HK-2 cells were treated with Stx1 B subunits on ice for 1 h. The cells were subsequently washed and incubated with 13C4, an anti-Stx1 monoclonal antibody, on ice for 30 min. After centrifugation, the cells were washed and incubated with fluorescein isothiocyanate (FITC)-conjugated anti-mouse IgG antibody for 30 min. After washing, the cells were subjected to fluorescence-activated cell sorter (FACS) analysis for membrane Gb_3 expression. The data shown are the means ± SEM for three independent experiments.

tants were collected and stored at −80°C until they were analyzed. The Bio-Plex Pro Human Cytokine Standard Group 1 27-Plex kit was purchased from Bio-Rad Laboratories (Hercules, CA) and used according to the manufacturer's instructions. A series of eight standards ranging in concentration from 1.95 to 32,000 pg/ml was included in each assay. Samples from three independent experiments were analyzed in triplicate and graphed using GraphPad Prism. The data are expressed as means of fold induction ± standard errors of the mean (SEM). Statistical significance was assessed at a P value of <0.05 by one-way ANOVA with Dunnett's posttest using Graphpad Prism version 5 (Graphpad Software, La Jolla, CA).

Western blot analysis. HK-2 cells were treated with 75 pg/ml Stx1 or Stx2, 100 μM thapsigargin (ER stress positive control), or 100 μM doxorubicin HCl (apoptosis positive control) for various times. Cells were harvested and lysed at 4°C in modified radioimmunoprecipitation assay (RIPA) buffer (1.0% Nonidet P-40, 1.0% sodium deoxycholate, 150 nM NaCl, 50 nM Tris-HCl [pH 7.5], 0.25 mM sodium pyrophosphate, sodium vanadate, and sodium fluoride [2.0 mM each], 10 mg of aprotinin/ml, 1.0 mg of leupeptin and pepstatin/ml, and 200 mM phenylmethylsulfonyl fluoride). Extracts were collected and cleared by centrifugation at 15,000 × g for 10 min, and the protein concentration was determined using the D*C* Protein Assay kit (Bio-Rad). Equal amounts of protein (100 μg per lane) were separated by SDS-PAGE using 4 to 20% acrylamide gels and transferred to nitrocellulose membranes, which were blocked with 5% nonfat milk prepared in Tris-buffered saline (TBS)-Tween 20 (200 mM Tris [pH 7.6], 1.38 M NaCl, 0.1% Tween 20) and incubated overnight at 4°C with primary antibodies specific for phospho-IRE1 (Novus Biologicals, Littleton, CO), ATF-6, phospho-PERK, total PERK, BiP, CCAAT/enhancer-binding protein (C/EBP) homologous protein (CHOP), PARP, caspase 3, caspase 8, and actin (Cell Signaling Technology, Inc., Danvers, MA) in 5% bovine serum albumin made with TBS-0.1% Tween 20. The membranes were then incubated with secondary antibodies (horseradish peroxidase-labeled anti-rabbit or anti-mouse antibodies; Cell Signaling Technology, Inc., Danvers, MA) for 1 h at room temperature. Bands were visualized using the Western Lightning Chemiluminescence System (NEN-Perkin Elmer, Boston, MA). The intensities of the protein bands captured on autoradiography film were quantified using Image J software (NIH, Bethesda, MD). The fold induction was calculated as treated protein band intensity values divided by untreated control protein band intensity values after normalizing for loading controls. The data shown are from at least three independent experiments. Statistical significance was assessed at a P value of <0.05 by one-way ANOVA with Dunnett's posttest using Graphpad Prism version 5 (Graphpad Software, La Jolla, CA).

RESULTS

HK-2 cells maintain high levels of membrane-associated toxin receptor expression. Renal tubular epithelial cells may be targets of Stxs early in disease progression. Gb_3 is the sole receptor characterized for all Stxs causing D^+HUS, and studies designed to examine renal Gb_3 expression *in situ* have shown that renal tubules express abundant Gb_3. Therefore, using an indirect immunofluorescence assay and flow cytometry, we examined Gb_3 expression by HK-2 cells (Fig. 1). It was determined that 95.6% ± 0.8% of the gated HK-2 cell population expressed Gb_3 on their surfaces. Gb_3 was not detected on cells treated with an isotype-matched primary antibody (isotype control; 1.1% ± 0.8%). These data suggest that, in keeping with studies examining renal Gb_3 expression, HK-2 cells maintain high membrane expression of the Stx receptor *in vitro*.

HK-2 cells are differentially sensitive to killing by Stx1 and Stx2. While primary human renal epithelial cells are sensitive to the cytotoxic effects of Stxs *in vitro*, Stx2 is more likely to lead to life-threatening extraintestinal complications. Therefore, we compared the cytotoxic effects of Stx1 and Stx2 on HK-2 cells. The cells were exposed to various concentrations of Stx1 or Stx2 for 3 different times (Fig. 2). The percent cell survival following toxin treatments was calculated in comparison to untreated control cells. Both Stx1 and Stx2 killed HK-2 cells in a dose-dependent fashion over the monitored time course; however, we noted significant differences in the kinetics and extents of cell death caused by the toxins at the various toxin concentrations. Treatment with Stx1 resulted in a more rapid onset of cell death than treatment with Stx2, with 35% and 58% of cells surviving following 24-h treatment with the

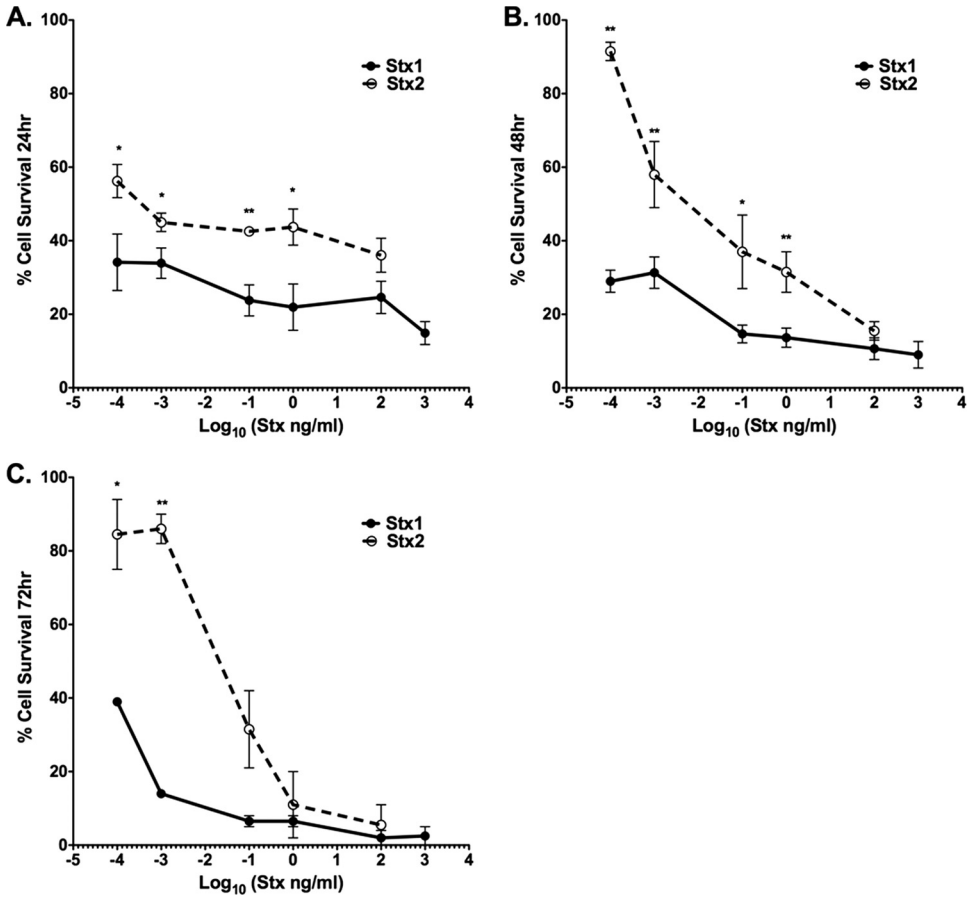

FIG. 2. Cytotoxic effects of Stx1 and Stx2 on HK-2 cells. HK-2 cells (5×10^4 cells per well) were incubated with different concentrations of either Stx1 or Stx2, as indicated. After incubation for 24 h (A), 48 h (B), or 72 h (C), viable-cell numbers were estimated by MTT assay. The graphs depict percent cell viability compared to untreated cells and represent the means ± SEM of three independent experiments. The asterisks denote significant differences between cells stimulated with Stx1 and Stx2 (*, $P < 0.05$; **, $P < 0.01$).

lowest dose (100 fg/ml) of either Stx1 or Stx2, respectively (Fig. 2A). With the toxin dose range used in this comparative study, cell viability did not appear to significantly change over time in response to Stx1, with cell survival remaining at or below 40% at all three time points. HK-2 cells were significantly less sensitive to Stx2 than to Stx1, as evidenced by reduced cell killing at all time points examined (Fig. 2A to C). The estimated 50% cytotoxic dose (CD_{50}) values for HK-2 cells treated with Stx1 or Stx2 are shown in Table 1.

Vero cells are used because they are highly sensitive to the cytotoxic action of Stxs. Therefore, using the viability indicator dye MTT, we compared the sensitivities of HK-2 cells and Vero cells to both Stx1 and Stx2 (Fig. 3). The percent cell survival following toxin treatments was calculated in comparison to untreated control cells. Both Vero and HK-2 cells responded to Stx1 and Stx2 in a dose-dependent manner at all monitored time points. The estimated CD_{50} for Vero cells exposed to Stx1 at the 24-h time point is ~800 pg/ml, and the CD_{50} for HK-2 cells is <100 fg/ml at the same time point (Table 1). We did not achieve 50% cytotoxicity in Vero cells treated with Stx2 at 24 h with the chosen dose range; however, the estimated CD_{50} for HK-2 cells at this time point is ~300 pg/ml (Table 1). Vero and HK-2 cells are similarly sensitive to Stx1 and Stx2 48 h after exposure; however, Stx1 appears to be more cytotoxic than Stx2 for both cell types (Fig. 3C and D). Despite HK-2 cells appearing to be more sensitive to the toxins at 24 h, by 72 h, Vero cells are highly sensitive to Stx1 and Stx2, with both toxins killing 100% of the Vero cells at all monitored doses. In contrast, a subset of HK-2 cells appears to have survived the cytotoxic effect, particularly the effect of low doses of Stx2 (Fig. 3E and F). Although we have not characterized the HK-2 cell subpopulation that survived toxin exposure, given the high replication rate of HK-2 cells in complete medium, the most likely explanation for increases in percent cell survival over time following Stx2 exposure is replication of cells that survived toxin challenge.

TABLE 1. CD_{50} values for HK-2 and Vero cells

Time (h)	CD_{50}			
	HK-2 cells		Vero cells	
	Stx1	Stx2	Stx1	Stx2
24	<100 fg/ml	300 fg/ml	800 pg/ml	>100 ng/ml
48	<100 fg/ml	6 pg/ml	300 fg/ml	2 ng/ml
72	<100 fg/ml	20 pg/ml	<100 fg/ml	<100 fg/ml

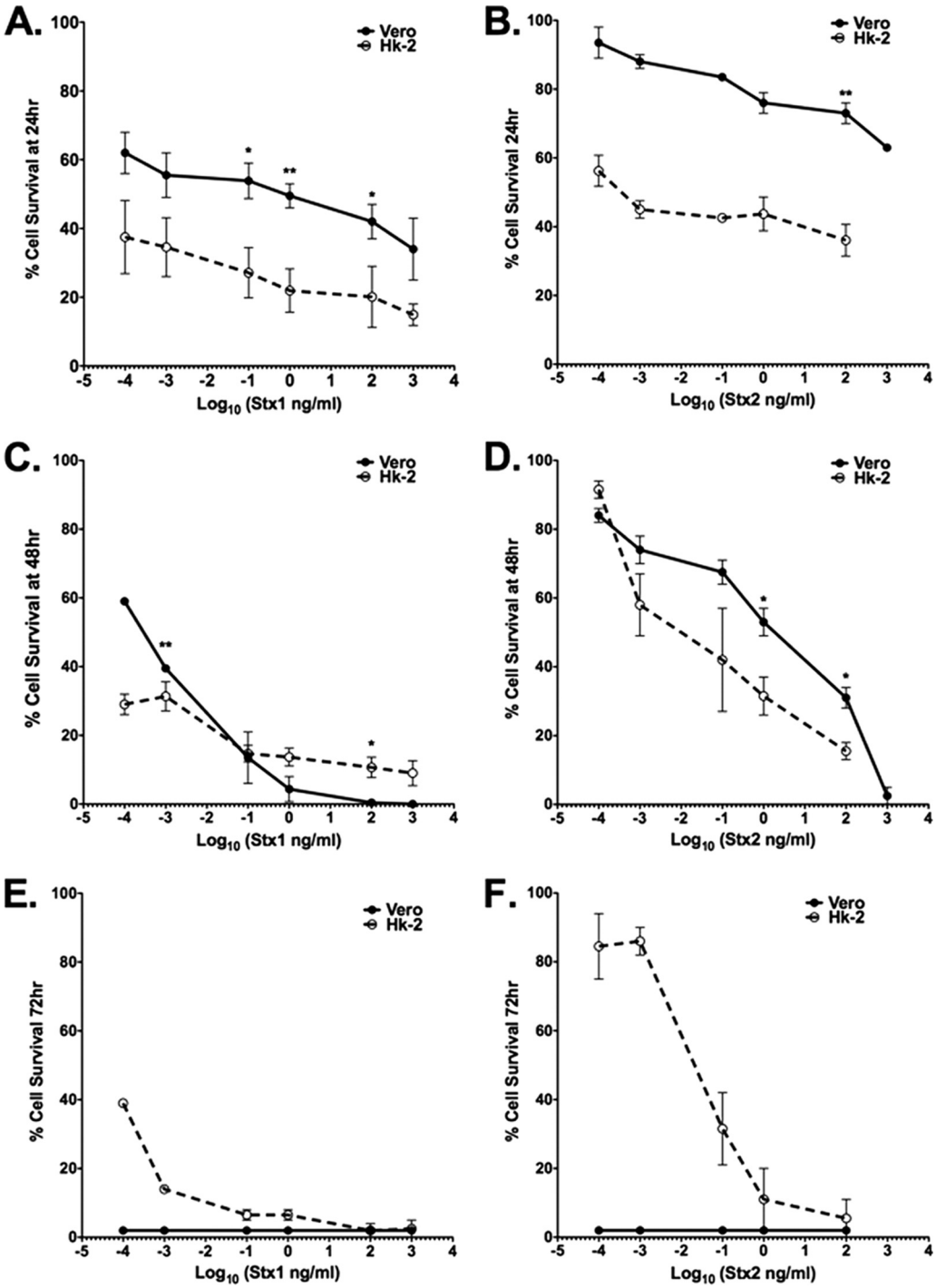

FIG. 3. Cytotoxic response of Vero cells to Stx1 or Stx2 versus that of HK-2 cells. Vero or HK-2 cells (5×10^4 cells per well) were incubated with different concentrations of either Stx1 or Stx2, as indicated. After incubation for 24 h (A and B), 48 h (C and D), or 72 h (E and F), viable-cell numbers were estimated by MTT assay. The graphs depict percent cell viability compared to untreated cells and represent the means ± SEM of three independent experiments. Vero cell and HK-2 cell cytotoxicities are denoted by solid lines and dashed lines, respectively. The asterisks denote significant differences between Vero and HK-2 cells (*, $P < 0.05$; **, $P < 0.01$).

Shiga toxin B subunits translocate to lysosomal and ER compartments in HK-2 cells. Following binding to Gb_3, Stxs enter cells via receptor-mediated endocytosis and utilize retrograde transport to access the ER lumen (44). To study the intracellular routing of Stxs in HK-2 cells, we used confocal fluorescence microscopy with fluorescently labeled Stx1 B subunits (Fig. 4). Cells were stained with Lyso-Tracker (red) or ER-Tracker (blue) live-cell-staining dyes and subsequently exposed to Stx1 B subunits conjugated with Alexa 488 (green) for the indicated times. Stx1 B subunits rapidly trafficked to both

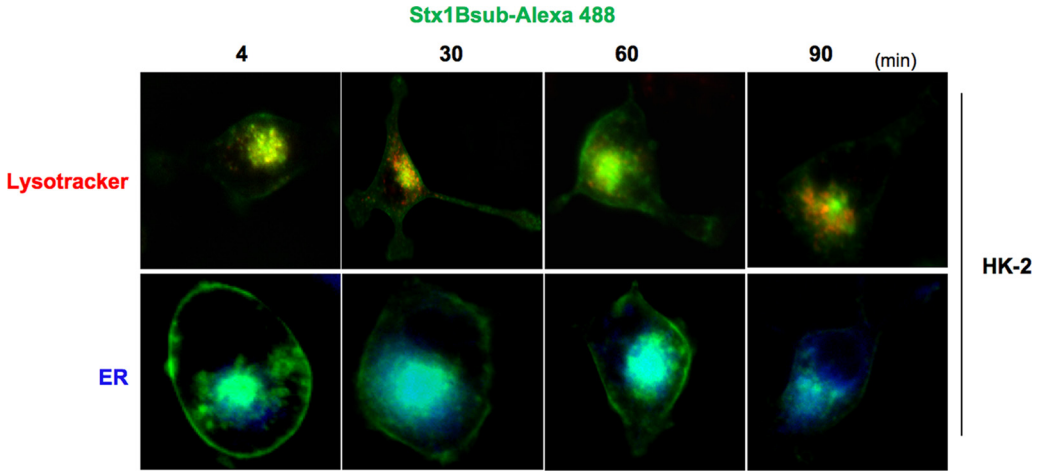

FIG. 4. Stx1 B subunit-Alexa 488 trafficking in HK-2 cells. HK-2 cells were treated with 100 nM Lyso-Tracker (red) or 60 nM ER-Tracker (blue) live-cell-staining dyes for detection of the lysosomal compartment and endoplasmic reticulum, respectively. Subsequently, the cells were stimulated with complete medium containing 100 ng/ml Stx1 B-Alexa 488 (green) for the indicated times. A single confocal optical section through the middle of the majority of cells in the field of view was taken for red, blue, and green emission channels simultaneously using a Stallion Digital imaging station. The presence of yellow or light-blue fluorescence in the merged images indicates toxin colocalization. The images are representative of two independent experiments. All data within each experiment were collected at identical settings.

lysosomal and ER compartments. Toxin was routed to the lysosome of HK-2 cells within 4 min, as indicated by the colocalization of the red and green dyes in merged images, producing yellow fluorescence. Simultaneously, Stx1 B subunits were routed to the ER compartments of HK-2 cells, as indicated by the light-blue fluorescence formed by blue and green dyes in merged images. Stx1 B subunit routing to the ER was noted as early as 4 min after treatment, and maximal ER localization was noted 60 min after Stx1 B subunit exposure. Use of fluorescently labeled Stx2 B subunits yielded similar trafficking data within HK-2 cells (data not shown). The sensitivity of HK-2 cells to Stxs may correlate with efficient intracellular routing to the ER. The observation that some portion of internalized toxin B subunits were routed to HK-2 cell lysosomes suggests that some cells may be able to survive toxin exposure by diverting greater amounts of internalized toxins into the lysosomal degradation pathway.

Cytokine and chemokine expression elicited by Stx1 and Stx2 treatment of HK-2 cells. Stxs trigger the release of cytokines and chemokines from epithelial and myeloid cells. To better understand the response of HK-2 cells to Stxs, we analyzed the expression of the proinflammatory cytokines TNF-α and IL-1β and the chemokines IL-8 (CXCL8), MIP-1α (CCL3), and MIP-1β (CCL4) at both the mRNA and protein levels (Fig. 5). Stx1 treatment elicited a modest and delayed increase in TNF-α mRNA expression, peaking at ~6-fold increase 4 h after toxin exposure. In contrast, Stx2 treatment induced a rapid increase in TNF-α mRNA (~200-fold) detected 15 min after toxin exposure. TNF-α mRNA levels then declined by 30 min and began to increase to levels ~100-fold higher than those in control cells by 120 min. It is important to note that in the presence of growth factors in complete medium (see Materials and Methods), HK-2 cells expressed high basal levels of cytokine and chemokine proteins. Despite basal levels of TNF-α protein expression and despite the capacity of the toxins to increase TNF-α mRNA production, neither Stx1 nor Stx2 induced the expression of TNF-α protein above untreated-control levels (Fig. 5A). There was an increase in the fold induction of IL-1β mRNA with both Stx1 and Stx2 treatments. Similar to the TNF-α transcriptional response, Stx1 minimally induced IL-1β transcripts, peaking at ~5-fold by 90 min, while Stx2 induced a maximal ~4,000-fold increase in IL-1β transcripts 30 min after treatment. Despite the detection of IL-1β transcripts after treatment with Stx1 and Stx2, IL-1β protein was not detected in cell supernatants, including untreated control cells (Fig. 5B).

Neutrophils have been reported to play a role in the development of D^+HUS (5). Therefore, we examined the ability of HK-2 cells to produce the major neutrophil chemoattractant IL-8 after exposure to Stx1 or Stx2. Stx1 did not elicit IL-8 mRNA or protein from HK-2 cells above untreated-control levels. In contrast, Stx2 triggered a 40-fold increase in IL-8 mRNA at 30 min, but protein levels were reduced relative to untreated controls (Fig. 5C). MIP-1α and MIP-1β are chemoattractants that primarily recruit macrophages to sites of infection and may play an important role in the pathogenesis of D^+HUS (25). Therefore, we examined the ability of HK-2 cells to produce MIP-1α and MIP-1β in response to Stx1 or Stx2. Stx1 was unable to generate MIP-1α or MIP-1β mRNA above control levels. In Stx1-treated cells, MIP-1α and MIP-1β proteins were reduced compared to untreated controls. In contrast to Stx1, Stx2 exposure triggered the upregulation of MIP-1α and MIP-1β at both the mRNA and protein levels (Fig. 5D and E). Thus, Stx2 appeared to be uniquely capable of upregulating the production and release of MIP-1α and MIP-1β by HK-2 cells *in vitro*. The upregulation of MIP-1α and MIP-1β may facilitate the recruitment of macrophages and neutrophils into sites of renal tubular damage and further exacerbate tissue damage.

The ER stress response is differentially induced after Stx1 or Stx2 exposure in HK-2 cells. The unfolded-protein response (UPR) is a "quality control" mechanism that has evolved to

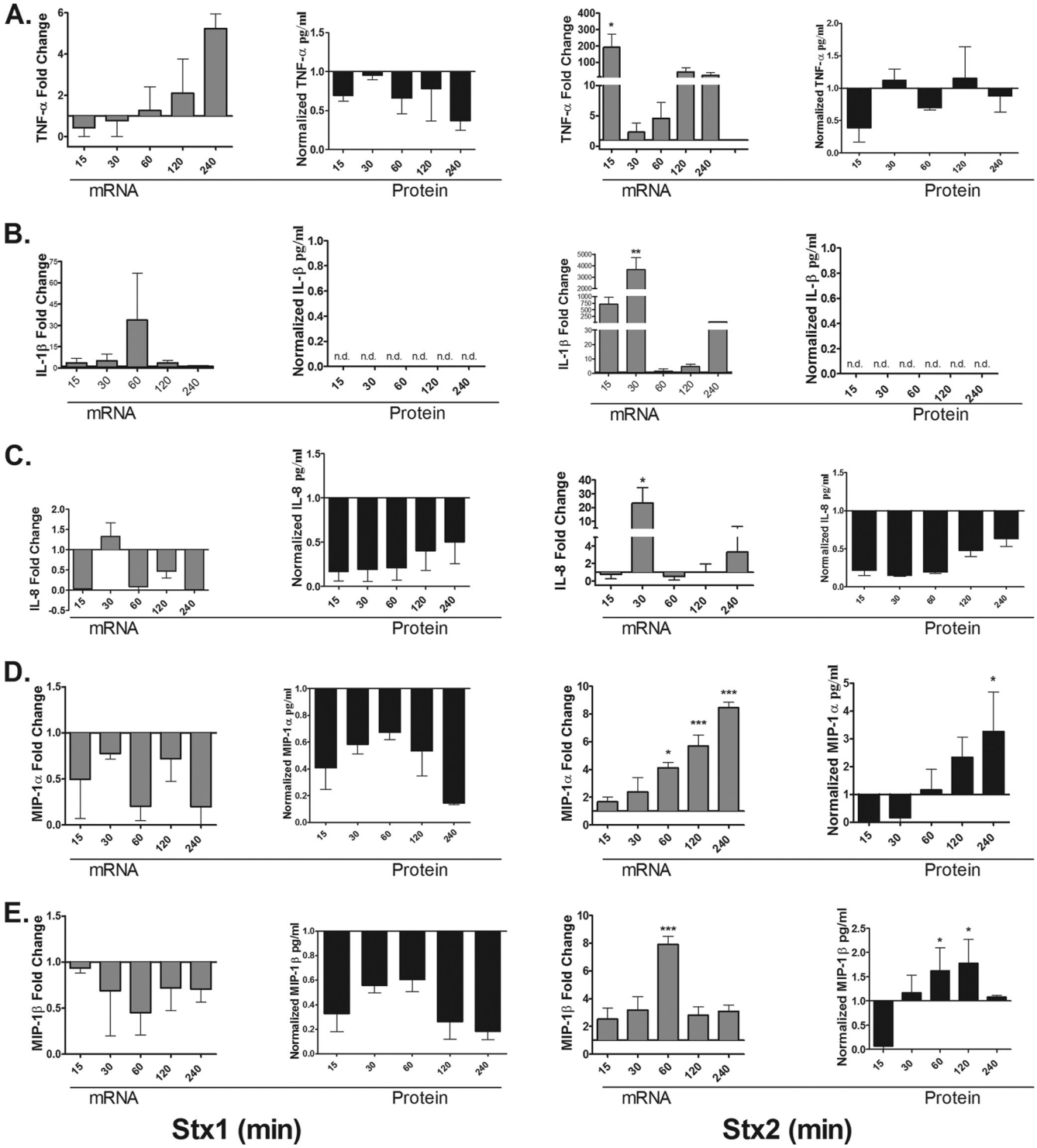

FIG. 5. Cytokine and chemokine production elicited by Stx1 and Stx2 treatment of HK-2 cells. HK-2 cells were stimulated with 75 pg/ml of either Stx1 or Stx2 for 15, 30, 60, 120, or 240 min. Total RNA was isolated, DNase treated, and cDNA synthesized. Quantitative real-time PCR was performed with primers specific for TNF-α (A), IL-1β (B), IL-8 (C), MIP-1α (D), MIP-1β (E), and the internal control GAPDH. Relative expression was calculated using the ΔC_T method and expressed as fold change relative to untreated-control levels (gray bars). The data were derived from at least two independent experiments. Cell supernatants were collected and analyzed for TNF-α, IL-1β, IL-8, MIP-1α, and MIP-1β proteins as described in Materials and Methods (black bars). The data shown are the mean fold change ± SEM derived from three independent experiments. Statistical significance was calculated using one-way ANOVA (*, $P < 0.05$; **, $P < 0.01$; ***, $P < 0.001$).

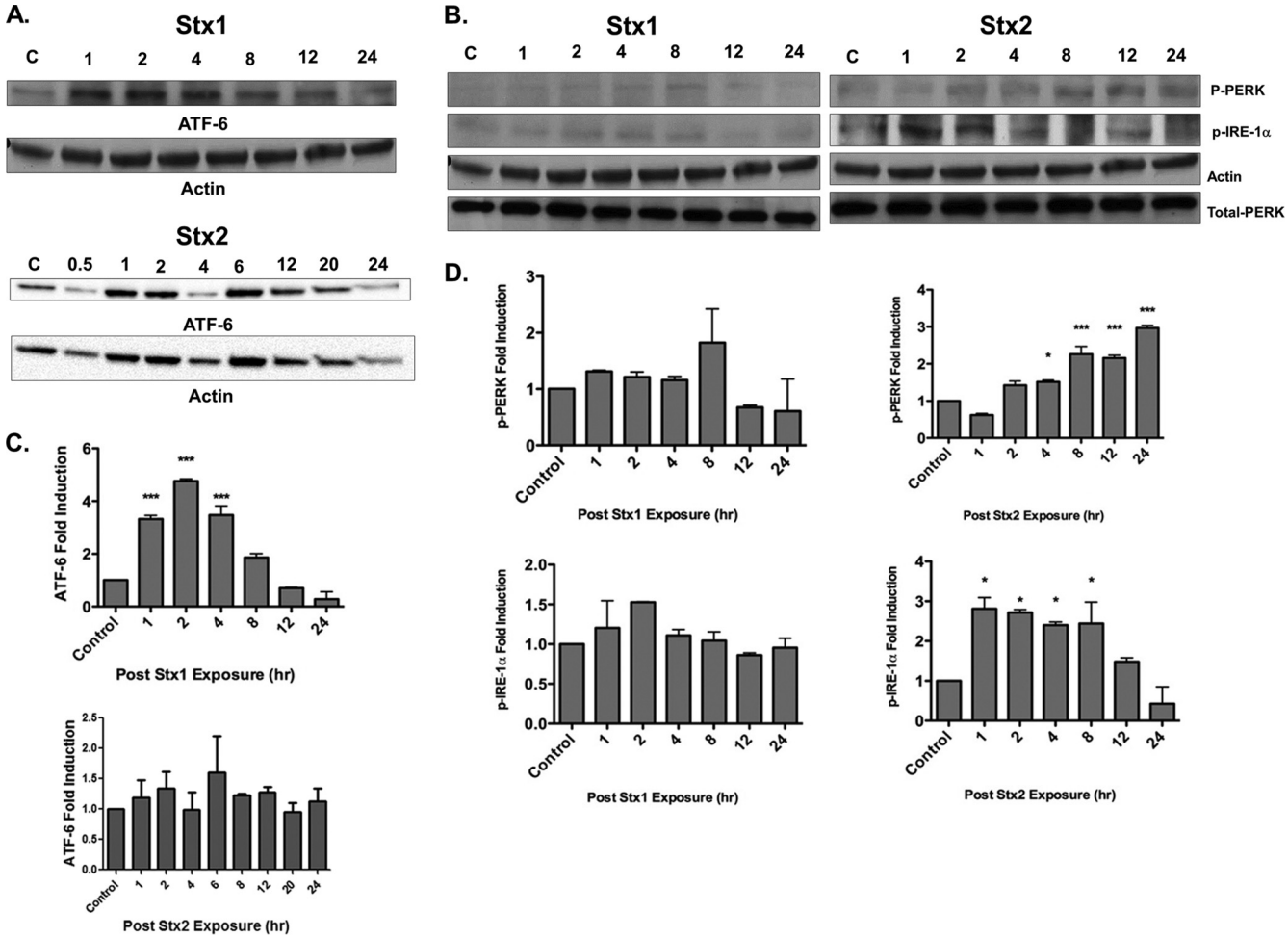

FIG. 6. UPR sensors are differentially activated after Stx1 or Stx2 exposure in HK-2 cells. (A and B) HK-2 cells were stimulated with 75 pg/ml Stx1 or Stx2, and at the indicated time points, cells were lysed and whole-cell lysates (100 μg/well) were subjected to SDS-PAGE (4% to 20%) and probed using antibodies specific for the activated forms of the UPR signaling molecules ATF6 (50 kDa) (A), phospho-PERK (170 kDa) (B), and phospho-IRE1α (110 kDa). The blots shown are characteristic of at least three independent experiments. (C and D) Mean densitometric readings of Western blot band intensities from three independent experiments. The data are expressed as means plus SEM; statistical significance was calculated using one-way ANOVA (*, $P < 0.05$; ***, $P < 0.001$) compared to control untreated cells.

detect the presence of unfolded or misfolded proteins within the ER lumen (10, 20). Failure to correct protein folding and restore normal anterograde protein transport/secretion pathways leads to ER stress or prolonged signaling through the UPR and the initiation of apoptosis (4, 39). Three sensors located within the ER membrane detect the presence of unfolded proteins: the transcription factor ATF6, the protein kinase/endoribonuclease IRE1, and the protein kinase PERK. Activation of these sensors by proteolytic cleavage (ATF6) or phosphorylation (IRE1 and PERK) alters gene expression, in part by upregulating the expression of the transcriptional factor CHOP, which positively regulates the expression of chaperone genes and negatively regulates the antiapoptotic protein Bcl-2 (2). To investigate whether Stx1 and Stx2 exposure triggers the ER stress response in HK-2 cells, we analyzed ATF6, IRE1, and PERK activation by Western blot analyses. In the presence of Stx1, cleavage of ATF6 peaked (~5-fold) 2 h after toxin stimulation but returned to basal levels within 12 h. Unlike Stx1, the transcription factor ATF6 was not significantly cleaved in response to Stx2 over the monitored period (Fig. 6A and C). We did not detect a significant change in the phosphorylation of PERK or IRE1 sensors throughout the monitored time course following treatment of HK-2 cells with Stx1. Stx2 elevated both PERK and IRE1α phosphorylation after toxin exposure. Phospho-PERK levels began to rise 2 h after Stx2 exposure with maximal signal detected at 24 h (3-fold induction; $P < 0.001$). Levels of phospho-IRE1α peaked 1 h after exposure (3-fold induction; $P < 0.05$) and returned to basal levels by 24 h (Fig. 6B and D). Using thapsigargin as a positive inducer of the ER stress sensors phospho-IRE1α and ATF6, we found a 3.6-fold increase in the phosphorylation of IRE1α and a 1.6-fold increase in ATF-6 proteolysis (data not shown). Thus, Stx1 and Stx2 appear to activate nonoverlapping components of the ER stress response in HK-2 cells.

BiP is the major chaperone present in the ER lumen involved in the detection of misfolded proteins. BiP dissociates from the luminal portion of ATF6, IRE1, and PERK to bind misfolded proteins (20). Signaling through UPR sensors up-

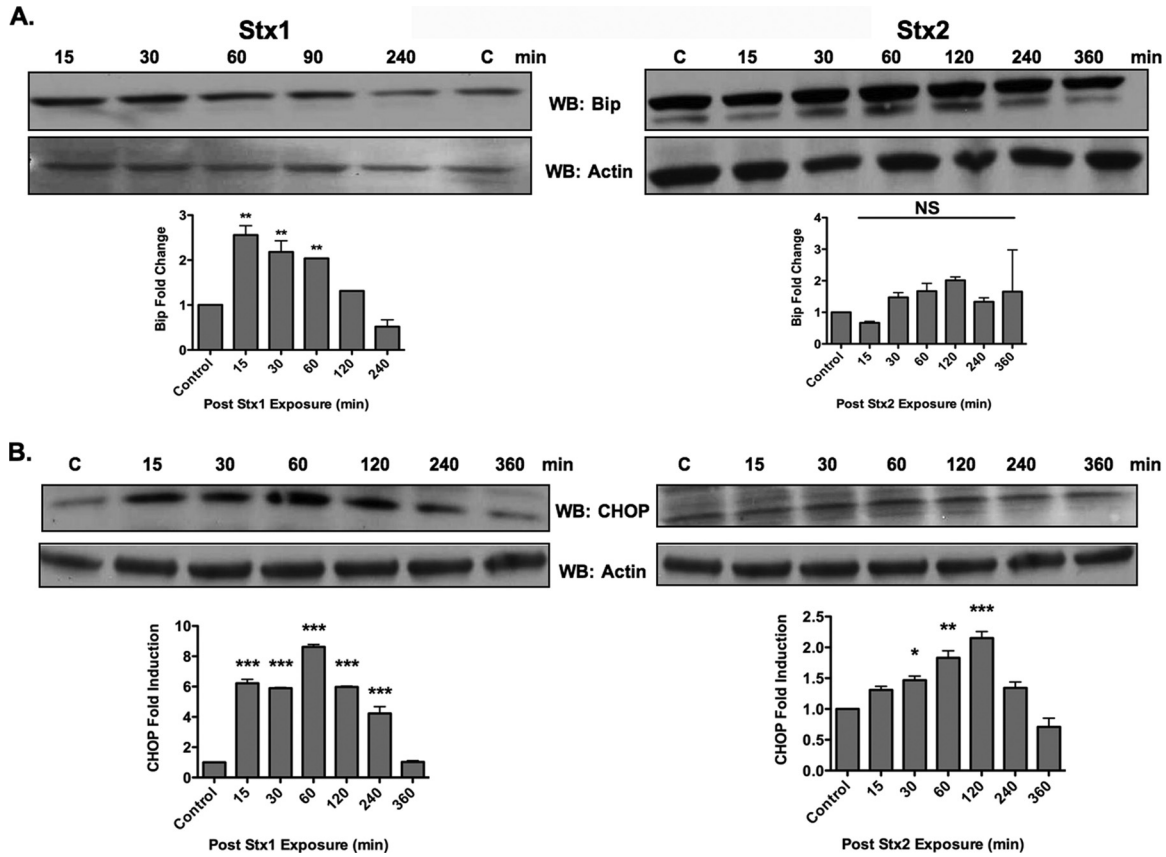

FIG. 7. The ER stress response is differentially activated in HK-2 cells in response to Stx1 or Stx2 treatment. HK-2 cells were exposed to 75 pg/ml Stx1 or Stx2, and at the indicated time points, cells were lysed and whole-cell lysates (100 μg/well) were subjected to SDS-PAGE (4% to 20%) and probed using antibodies specific for BiP (78 kDa) (A) and CHOP (28 kDa) (B). The blots shown are characteristic of three independent experiments. The bar graphs depict fold changes derived from mean densitometric readings of Western blot band intensities from three independent experiments. The data are expressed as means plus SEM, and statistical significance was calculated using one-way ANOVA. The asterisks denote significant differences compared to control cells (*, $P < 0.05$; **, $P < 0.01$; ***, $P < 0.001$; NS, not significant).

regulates the expression of BiP. To examine the functionality of ER stress triggered by Stx1 and Stx2 in HK-2 cells, we assessed the effect of toxin treatment on BiP expression. Stx1 significantly upregulated BiP protein levels. Fifteen minutes after exposure to Stx1, HK-2 cells had ~3-fold induction in BiP protein levels, which returned to basal levels within 4 h (Fig. 7A). We did not detect significant increases in BiP protein levels following Stx2 treatment, even when the time course was extended to 6 h. The UPR also increases expression of the transcription factor CHOP (2). We therefore investigated the effects of Stx1 and Stx2 on CHOP protein levels expressed by HK-2 cells. CHOP protein levels showed maximal increase 60 min after intoxication with Stx1, peaking at ~9-fold increase compared to untreated control cells (Fig. 7B). Stx2 treatment did not upregulate CHOP expression to the same extent as Stx1, as maximal fold induction peaked at 2.1 ± 0.1. CHOP expression induced by Stx2 treatment was significantly upregulated compared to untreated control cells. Collectively, these data suggest that Stx1 and Stx2 differentially induce the ER stress response in HK-2 cells.

Stx1 and Stx2 treatment induces caspase 3-independent PARP cleavage. Stx1 and Stx2 treatment of HK-2 cells induced PARP cleavage, although Stx1 cleaved PARP more quickly and to a greater extent than Stx2 (Fig. 8A and B). The rapid activation of caspase 8 and 3 has emerged as a key element in Stx-induced apoptosis (30), and PARP is a known substrate of caspase 3 (53). Therefore, we examined the effect of Stx1 or Stx2 treatment on the activation of caspase 3 and 8 in HK-2 cells. We were unable to detect procaspase 3 cleavage following treatment of HK-2 cells with either Stx1 or Stx2 throughout the monitored time course (Fig. 8A). Doxorubicin HCl, a positive control for procaspase 3 cleavage, showed a 3-fold increase in cleaved caspase 3 levels over untreated-control levels (Fig. 8C). Treatment of HK-2 cells with Stx1 did not significantly cleave procaspase 8 (Fig. 8A and B). In contrast, Stx2 significantly cleaved procaspase 8 ($P < 0.001$), with maximal cleavage detected 8 h after toxin exposure (Fig. 8A and B). Collectively, these data show that Stx1 and Stx2 may cleave PARP independently of procaspase 3 cleavage. Furthermore, Stx2 selectively activates caspase 8 in HK-2 cells.

DISCUSSION

Renal proximal epithelial cells express abundant Gb_3 *in situ* and have been implicated as targets of the action of Stxs. For example, Karpman et al. used human renal cortical

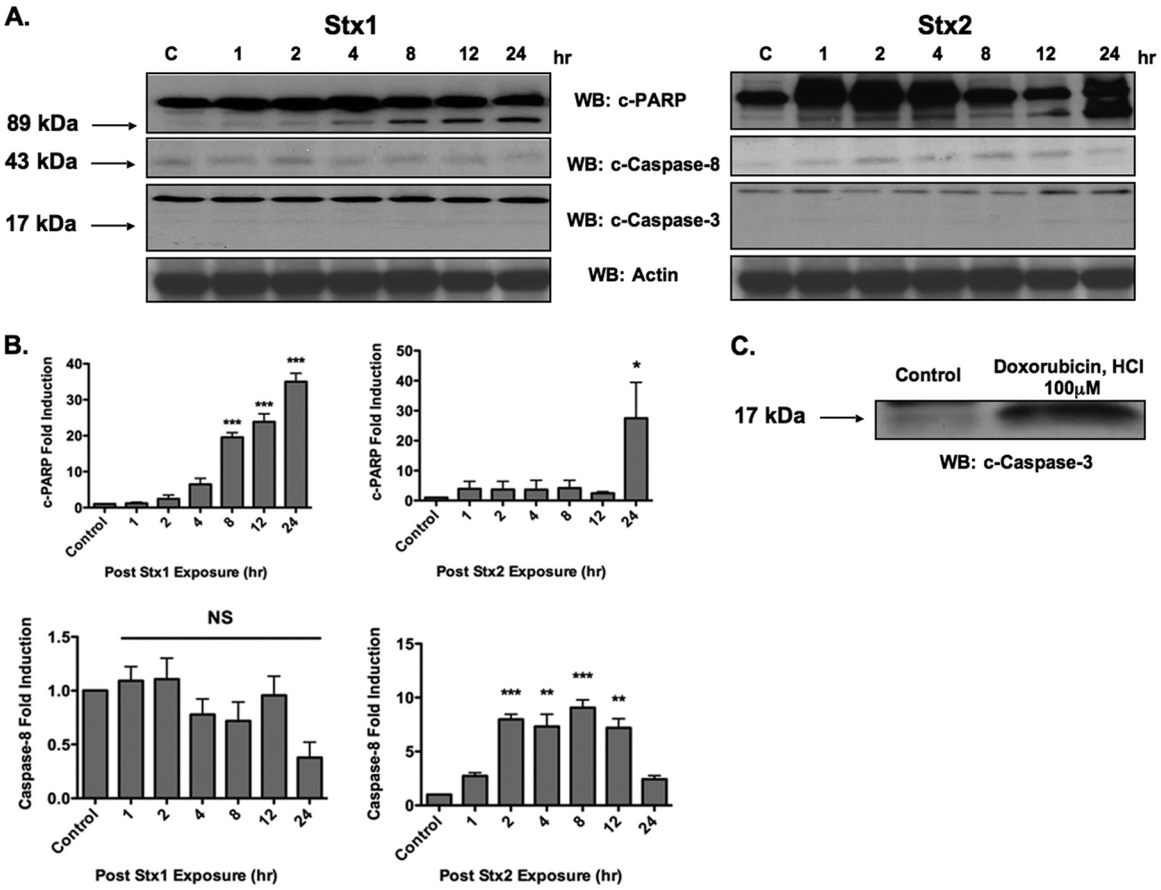

FIG. 8. Stx1 and Stx2 treatment induces caspase 3-independent PARP cleavage. (A) HK-2 cells were stimulated with 75 pg/ml Stx1 or Stx2, and at the indicated time points, cells were lysed and whole-cell lysates (100 μg/well) were subjected to SDS-PAGE (4% to 20%) and probed using antibodies specific for cleaved PARP (c-PARP; 89 kDa), caspase 3 (17 kDa), and caspase 8 (43 kDa). The blots shown are characteristic of three independent experiments. WB, Western blotting. (B) Fold changes in PARP and procaspase 8 cleavage derived from mean densitometric readings of Western blot band intensities from three independent experiments. The data are expressed as means plus SEM, and statistical significance was calculated using one-way ANOVA. The asterisks denote significant differences compared to control cells (*, $P < 0.05$; **, $P < 0.01$; ***, $P < 0.001$; NS, not significant). (C) HK-2 cells were stimulated with doxorubicin HCl as a positive control for apoptosis induction for 6 h, subjected to SDS-PAGE, and probed using antibodies specific for caspase 3.

epithelial cells and a renal carcinoma cell line to investigate the cytotoxic effects of Stxs (23). Stxs induced apoptosis in both cell types, as evidenced by nuclear fragmentation, DNA laddering, and the presence of terminal deoxynucleotidyltransferase-mediated dUTP-biotin nick end labeling (TUNEL)-positive cells. We showed that HK-2 cells maintain high levels of Gb_3 expression *in vitro* and are sensitive to Stx1 and Stx2. Given epidemiologic studies suggesting that infections with Stx2-producing *E. coli* strains are more likely to progress to D^+HUS (3, 24, 37), one might predict that HK-2 cells would be more sensitive to Stx2. We found the converse to be the case. HK-2 cells were sensitive to all doses of Stx1 at all time points tested ($CD_{50} < 0.1$ pg/ml). HK-2 cells were less sensitive to Stx2 and over time showed an upward trend in CD_{50} values, suggesting that a subpopulation of cells may have survived Stx2 exposure. Vero cells are widely used as the prototypical cell type for defining Stx cytotoxicity, and we compared Vero and HK-2 cell sensitivities to the toxins. The data highlight the importance of establishing experimental parameters in determining CD_{50}s. At 24 h, HK-2 cells were significantly more sensitive to Stxs; by 48 h, the cells displayed similar dose-dependent cytotoxicity profiles; and at 72 h, Vero cell monolayers were completely destroyed while a subset of HK-2 cells appeared to have survived Stx2 challenge. Histopathologic examination of renal tissues from animals administered purified Stxs showed evidence of renal tubule regeneration (51), and the HK-2 cells that survived Stx2 challenge may represent this subpopulation. Other cell types have displayed differential sensitivity to Stxs. For example, Bauwens et al. (1) showed that a cell line derived from human umbilical veins was ~10 times more sensitive to killing by Stx1 than by Stx2, while microvascular endothelial cells were more sensitive to killing by Stx2. There are a number of factors that may influence cell susceptibility to Stxs, including levels of Gb_3 expression, biochemical characteristics of Gb_3 (e.g., fatty acid chain length and degree of hydroxylation), Gb_3 presentation at the membrane (e.g., lipid raft-associated expression), and mechanisms of toxin internalization and intracellular routing. Fluorescently labeled Stx1 B subunits have been exten-

sively employed to characterize Stx intracellular routing to different cellular compartments (11, 14). We showed that B subunits were routed to ER and lysosomal compartments in HK-2 cells. Rapid transport to the ER, with maximal fluorescence detected 60 min after Stx1 B subunit exposure, correlates with the sensitivity of HK-2 cells to killing by Stxs. The data showing that HK-2 cells route Stxs to lysosomes suggest that the subpopulation of cells surviving toxin exposure may direct a portion of internalized toxins into the lysosomal degradation pathway.

Hughes et al. (18) noted that primary human renal proximal tubule epithelial cells cultured *in vitro* for 24 h expressed basal levels of soluble TNF-α and IL-1 (84.2 ± 17.4 and 9.0 ± 1.4 ng/mg, respectively). Incubation of the cells with sublethal concentrations (0.01 to 0.1 pg/ml) of Stx1 for 4 h failed to increase cytokine expression above basal levels, although exposure to Stx1 for 24 to 48 h resulted in 2- to 4-fold increases in TNF-α and IL-1 protein expression. Increases in cytokine protein expression were accompanied by greater increases in TNF-α and IL-1 transcripts. We also detected basal expression of soluble TNF-α (~2.0 pg/ml) in supernatants collected from HK-2 cells. The treatment of HK-2 cells with Stx1 or Stx2 for up to 4 h increased TNF-α and IL-1β transcript levels without concomitant significant increases in protein expression. Thus, prior to the onset of extensive cell death, neither primary cells nor HK-2 cells appear to be significant producers of TNF-α or IL-1β when exposed to Stxs *in vitro*. Stxs did not appear to induce the expression of the neutrophil chemoattractant IL-8. With the exception of a single time point following exposure to Stx2 for 30 min, we did not detect significant elevations in IL-8 mRNA levels, and IL-8 protein levels were reduced, albeit in a statistically nonsignificant manner, compared to basal IL-8 expression. However, HK-2 cells released the macrophage chemoattractants MIP-1α and MIP-1β in response to Stx2 treatment, but not in the presence of Stx1. Keepers et al. (25) used a murine model of Stx-mediated renal damage to show that macrophages were recruited to the kidneys of mice injected with Stx2 with or without lipopolysaccharides (LPS), in association with increased renal production of chemoattractants, including MIP-1α. Neutralizing antibodies against MIP-1α decreased macrophage infiltration and fibrin deposition within the renal vasculature. These findings suggest a role for infiltrating macrophages in D^+HUS but do not clarify which cell type(s) secretes chemokines in response to Stxs. Our data suggest that Stx2 is uniquely capable of triggering the production and release of MIP-1α and MIP-1β, and localized upregulation of chemokine production may facilitate the recruitment of activated immune cells, such as macrophages, into sites of initial tissue damage. HK-2 cells express tissue factor constitutively, and Stx1 induces the expression of cell surface tissue factor in a dose- and time-dependent manner (35). Toxin-mediated renal tubular damage may activate the coagulation system, leading to the formation of platelet-fibrin microthrombi. Macrophages and macrophage cell lines are known to produce tissue factor and cytokines in response to Stxs (34). Thus, infiltrating macrophages may further exacerbate inflammation, thrombogenesis, and tissue damage.

The mechanism(s) by which Stxs induce apoptosis in HK-2 cells has not been well characterized. Wilson et al. (56) showed that HK-2 cells were sensitive to Stx2, undergoing apoptosis, as assessed by PARP cleavage and nuclear fragmentation. The silencing of expression of the proapoptotic factor Bak decreased PARP cleavage and protected HK-2 cells from apoptosis, suggesting that Stxs trigger signaling through the intrinsic or mitochondrion-mediated apoptosis pathway. Stxs induce apoptosis in the THP-1 cell line through activation of the UPR and prolonged ER stress signaling (31). The ER is the site of protein folding and posttranslational modification, trafficking of proteins to various locations, and intracellular Ca^{2+} storage (2, 41). Protein folding and processing are monitored by a series of "folding sensors" localized within the ER membrane: the transcriptional activator ATF6, the serine/threonine kinase PERK, and the kinase/endoribonuclease IRE1. The chaperone BiP dissociates from the sensors in the presence of unfolded or misfolded proteins, leading to kinase dimerization and activation and the transit of ATF6 to the Golgi apparatus for proteolysis and activation. The activated sensors initiate the UPR, a coordinated series of signaling events involving the attenuation of translation and the transcriptional activation of genes encoding proteins involved in protein folding and degradation. Thus, the UPR may result in decreased *de novo* protein synthesis and clearance of unfolded proteins from the ER lumen (41). However, prolonged UPR signaling leads to ER stress and the induction of apoptosis (4, 41). Therefore, we examined the capacity of Stxs to induce ER stress in HK-2 cells. Stx1 and Stx2 activated different and nonoverlapping UPR sensors. Stx1 induced ATF6 cleavage from the inactive 90-kDa form to the active 50-kDa fragment. Stx2 triggered the phosphorylation of the sensors PERK and IRE1α. Signaling for increased expression of the chaperone BiP appeared to be correlated with ATF6 activation, as Stx1 transiently, but significantly, upregulated BiP expression. ER stress-induced apoptosis is mediated in large part by the transcriptional factor CHOP. The ability of CHOP to induce apoptosis is dependent on the duration and degree of ER stress (19). CHOP is activated through PERK and ATF6 signaling and induces the expression of several proapoptotic factors. Stx1 induced a 9-fold increase in CHOP expression 1 h after intoxication compared to a 2.5-fold maximal increase in HK-2 cells exposed to Stx2. Thus, the increased sensitivity of HK-2 cells to Stx1 appears to be correlated with the effective activation of ATF6, leading to enhanced signaling through CHOP, while HK-2 cell survival following Stx2 challenge may be related to reduced ATF6 activation and the transient activation of ER stress. Additional studies will be required to explore the role of ER stress in HK-2 cell death and survival.

Despite differences in the ER stress response, both toxins triggered PARP cleavage. Caspase 3 is the major executioner caspase involved in PARP cleavage, and several studies have shown that Stxs activate caspase 3 in epithelial cells and cell lines (50). Thus, our inability to detect procaspase 3 cleavage in HK-2 cells treated with Stxs was unexpected. Calpains may cleave PARP in the absence of caspase activation (55), and preliminary data from our laboratory suggest that both Stx1 and Stx2 activate calpains in HK-2 cells. PARP may also be activated by proapoptotic mitochondrial

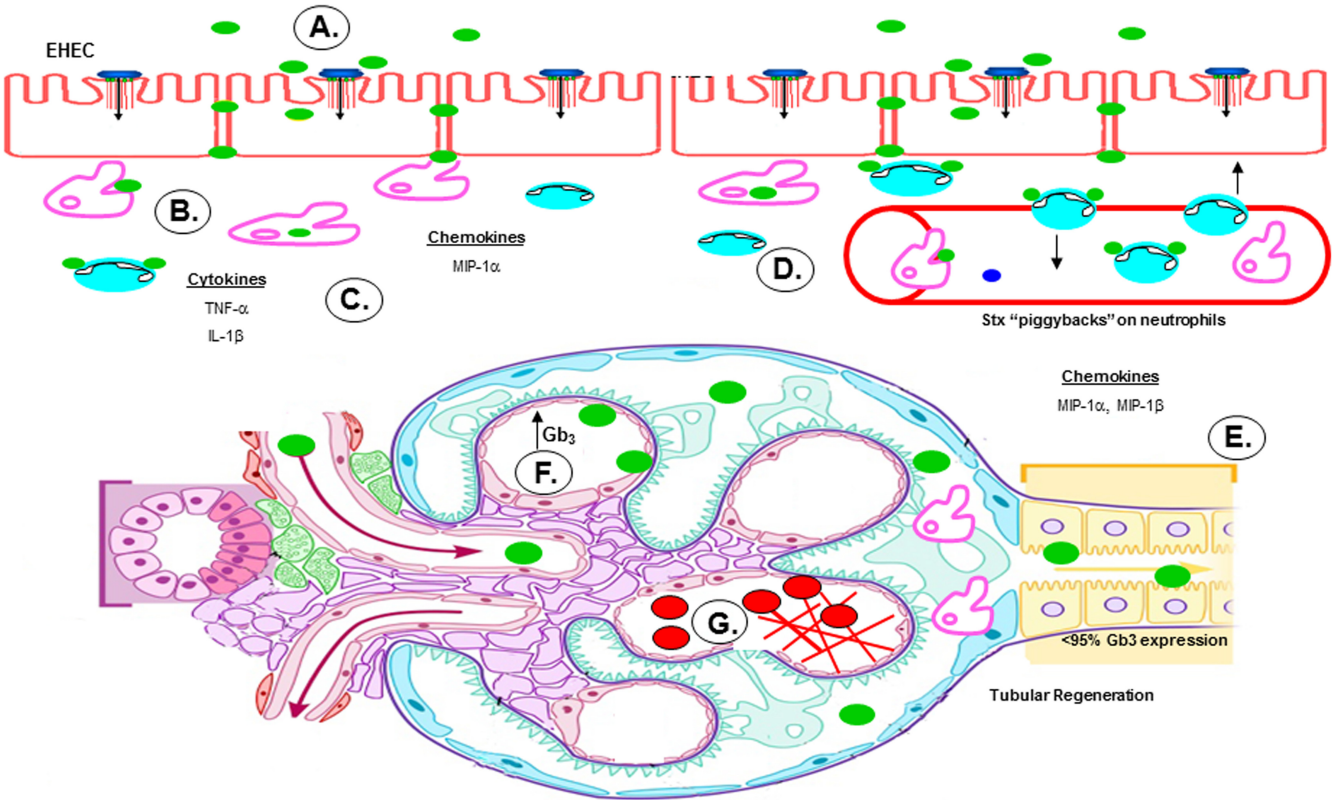

FIG. 9. Potential role of human proximal tubule epithelial cells in the pathogenesis of hemolytic uremic syndrome. (A) STEC adheres to the colonic epithelium. (B) The bacteria produce and release Stxs (green), which may gain access to the submucosa via transcytotic or paracellular mechanisms. (C) Stxs are internalized by resident tissue macrophages, inducing the production and secretion of proinflammatory cytokines and chemokines. Simultaneously, Stxs bind to and "piggyback" on neutrophils through circulation. (D) TNF-α and IL-1β upregulate expression of the Stx receptor on endothelial cells, resulting in increased vascular damage and systemic transport of Stxs in the blood. (E) Once in circulation, Stxs target the renal epithelium, which is rich in membrane-bound Gb_3. Renal proximal tubular epithelial cells are damaged, but a subpopulation of cells survive and, in response to Stx2, secrete both MIP-1α and MIP-1β, which in turn recruit inflammatory cells, such as macrophages and neutrophils, to sites of damage. (F) Activated macrophages secrete TNF-α and IL-1β, further sensitizing the microvascular endothelial cells. (G) Fibrin deposits build up in the microvasculature of the kidney, trapping circulating red blood cells and platelets. (Figure adapted from *Medical Illustrations*, Michal Komorniczak, with permission.)

intermembrane proteins released following the disruption of mitochondrial membranes, including apoptosis-inducing factor and endonuclease G (8). Stxs activate apoptotic signaling through the rapid activation of caspase 8 in several different cell types (13, 30). Our data suggest that Stx2 cleaves procaspase 8 in HK-2 cells while Stx1 fails to do so. Stx-induced activation of caspase 8 may lead to the activation of the Bcl-2 protein family member BID, which in turn translocates to the mitochondria to facilitate mitochondrial-membrane depolarization and the release of mitochondrial intermembrane constituents into the cytoplasm (29). These events trigger the formation of the apoptosome and the activation of procaspase 9, and caspase 9 then activates caspase 3. We detected minimal caspase 3 generation in Stx-treated HK-2 cells. Precisely how caspase 3 activation is disrupted is not known, but Fujii et al. (12) showed that Stx treatment of HeLa cells resulted in increased expression of XIAP, which blocks caspase 3 activation. Whether a similar pathway limiting apoptosis induction is operative in HK-2 cells requires additional scrutiny.

We used results gathered from *in vitro* and *in vivo* studies to derive a model for the role of renal epithelial cells in the pathogenesis of disease caused by STEC (Fig. 9). Following adherence to colonic epithelial cells, the bacteria produce Stxs (Fig. 9A). LPS from STEC (or from other intestinal flora) may gain access to the submucosa, as patients with STEC infections frequently possess elevated anti-STEC O-antigen antibody titers (38). Once within the lamina propria, the toxins encounter resident tissue macrophages and neutrophils (Fig. 9B). Toxin interaction with macrophages elicits the rapid expression and secretion of proinflammatory cytokines and chemokines (15, 16). TNF-α and IL-1β secreted by macrophages may exacerbate Stx-induced damage to colonic capillaries, releasing blood into the lumen of the intestine and creating portals of entry for Stxs and LPS into the bloodstream (Fig. 9C). Toxin binding to neutrophils may facilitate hematogenous spread and access to target organs (Fig. 9B and D) (5). The toxins may access the renal tubular epithelium via blood vessels supplying the tubules, although the precise mechanism is not known. Based on data presented here, Stx2 may selectively induce the expression of the chemokines MIP-1α and MIP-1β by proximal tubules of the human kidney (Fig. 9E). These chemokines recruit macrophages to sites of injury. Infiltrating macrophages may

produce cytokines and sensitize glomerular endothelial cells to Stxs by upregulating expression of membrane-bound Gb_3 (Fig. 9F). Microvascular damage progresses to the formation of fibrin deposits, which bind circulating red blood cells and platelets, leading to hemolytic anemia and thrombocytopenia (Fig. 9G).

ACKNOWLEDGMENTS

We thank Jane Miller and Rola Barhoumi for technical assistance and Cheleste Thorpe for the gift of reagents necessary to perform this study.

This work was supported by National Institutes of Health grant RO1 AI34530-14.

REFERENCES

1. **Bauwens, A., et al.** 2011. Differential cytotoxic actions of Shiga toxin 1 and Shiga toxin 2 on microvascular and macrovascular endothelial cells. Thromb. Haemost. **105:**515–528.
2. **Bernales, S., F. R. Papa, and P. Walter.** 2006. Intracellular signaling by the unfolded protein response. Annu. Rev. Cell Dev. Biol. **22:**487–508.
3. **Boerlin, P., et al.** 1999. Associations between virulence factors of Shiga toxin-producing *Escherichia coli* and disease in humans. J. Clin. Microbiol. **37:**497–503.
4. **Breckenridge, D. G., M. Germain, J. P. Mathai, M. Nguyen, and G. C. Shore.** 2003. Regulation of apoptosis by endoplasmic reticulum pathways. Oncogene **22:**8608–8618.
5. **Brigotti, M., et al.** 2008. Interactions between Shiga toxins and human polymorphonuclear leukocytes. J. Leukoc. Biol. **84:**1019–1027.
6. **Chaisri, U., et al.** 2001. Localization of Shiga toxins of enterohaemorrhagic *Escherichia coli* in kidneys of paediatric and geriatric patients with fatal haemolytic uraemic syndrome. Microb. Pathog. **31:**59–67.
7. **Cherla, R. P., S.-Y. Lee, P. L. Mees, and V. L. Tesh.** 2006. Shiga toxin 1-induced cytokine production is mediated by MAP kinase pathways and translation initiation factor eIF4E in the macrophage-like THP-1 cell line. J. Leukoc. Biol. **79:**397–407.
8. **Cho, B. B., and L. H. Toledo-Pereyra.** 2008. Caspase-independent programmed cell death following ischemic stroke. J. Invest. Surg. **21:**141–147.
9. **DeGrandis, S., H. Law, J. Brunton, C. Gyles, and C. A. Lingwood.** 1989. Globotetraosylceramide is recognized by the pig edema disease toxin. J. Biol. Chem. **264:**12520–12525.
10. **Ellgaard, L., and A. Helenius.** 2001. ER quality control: towards an understanding at the molecular level. Curr. Opin. Cell Biol. **13:**431–437.
11. **Falguières, T., et al.** 2001. Targeting of Shiga toxin B-subunit to retrograde transport route in association with detergent-resistant membranes. Mol. Biol. Cell **12:**2453–2468.
12. **Fujii, J., et al.** 2003. Rapid apoptosis induced by Shiga toxin in HeLa cells. Infect. Immun. **71:**2724–2735.
13. **Garibal, J., E. Hollville, B. Renouf, C. Tétaud, and J. Wiels.** 2010. Caspase-8-mediated cleavage of Bid and protein phosphatase 2A-mediated activation of Bax are necessary for Verotoxin-1-induced apoptosis in Burkitt's lymphoma cells. Cell Signal. **22:**467–475.
14. **Haicheur, N., et al.** 2000. The B subunit of Shiga toxin fused to a tumor antigen elicits CTL and targets dendritic cells to allow MHC class I-restricted presentation of peptides derived from exogenous antigens. J. Immunol. **165:**3301–3308.
15. **Harrison, L. M., C. van den Hoogen, W. C. E. van Haaften, and V. L. Tesh.** 2005. Chemokine expression in the monocytic cell line THP-1 in response to purified Shiga toxin 1 and/or lipopolysaccharides. Infect. Immun. **73:**403–412.
16. **Harrison, L. M., W. C. E. van Haaften, and V. L. Tesh.** 2004. Regulation of proinflammatory cytokine expression by Shiga toxin 1 and/or lipopolysaccharides in the human monocytic cell line THP-1. Infect. Immun. **72:**2618–2627.
17. **Hughes, A. K., P. K. Stricklett, and D. E. Kohan.** 1998. Cytotoxic effect of Shiga toxin-1 on human proximal tubule cells. Kidney Int. **54:**426–437.
18. **Hughes, A. K., P. K. Stricklett, and D. E. Kohan.** 1998. Shiga toxin-1 regulation of cytokine production by human proximal tubule cells. Kidney Int. **54:**1093–1106.
19. **Inagi, R.** 2009. Endoplasmic reticulum stress in the kidney as a novel mediator of kidney injury. Nephron Exp. Nephrol. **112:**e1–e9.
20. **Inagi, R., et al.** 2005. Involvement of endoplasmic reticulum (ER) stress in podocyte injury induced by excessive protein accumulation. Kidney Int. **68:**2639–2650.
21. **Jackson, M. P., R. J. Neill, A. D. O'Brien, R. K. Holmes, and J. W. Newland.** 1987. Nucleotide sequence analysis and comparison of the structural genes for Shiga-like toxin I and Shiga-like toxin II encoded by bacteriophages from *Escherichia coli* 933. FEMS Microbiol. Lett. **44:**109–114.
22. **Johannes, L., and W. Römer.** 2010. Shiga toxins—from cell biology to biomedical applications. Nat. Rev. Microbiol. **8:**105–116.
23. **Karpman, D., et al.** 1998. Apoptosis of renal cortical cells in the hemolytic-uremic syndrome: in vivo and in vitro studies. Infect. Immun. **66:**636–644.
24. **Kawano, K., M. Okada, T. Haga, K. Maeda, and Y. Goto.** 2008. Relationship between pathogenicity for humans and stx genotype in Shiga toxin-producing *Escherichia coli* serotype O157. Eur. J. Clin. Microbiol. Infect. Dis. **27:**227–232.
25. **Keepers, T. R., L. K. Gross, and T. G. Obrig.** 2007. Monocyte chemoattractant protein 1, macrophage inflammatory protein 1 alpha, and RANTES recruit macrophages to the kidney in a mouse model of hemolytic-uremic syndrome. Infect. Immun. **75:**1229–1236.
26. **Kiyokawa, N., et al.** 1998. Induction of apoptosis in normal human renal tubular epithelial cells by *Escherichia coli* Shiga toxins 1 and 2. J. Infect. Dis. **178:**178–184.
27. **Kodama, T., et al.** 1999. Induction of apoptosis in human renal proximal tubular epithelial cells by *Escherichia coli* verocytotoxin 1 in vitro. Med. Microbiol. Immunol. **188:**73–78.
28. **Koster, F. T., V. Boonpucknavig, S. Sujaho, R. H. Gilman, and M. M. Rahaman.** 1984. Renal histopathology in the hemolytic-uremic syndrome following shigellosis. Clin. Nephrol. **21:**126–133.
29. **Lee, M.-S., R. P. Cherla, D. Leyva-Illades, and V. L. Tesh.** 2009. Bcl-2 regulates the onset of Shiga toxin 1-induced apoptosis in THP-1 cells. Infect. Immun. **77:**5233–5244.
30. **Lee, S.-Y., R. P. Cherla, I. Caliskan, and V. L. Tesh.** 2005. Shiga toxin 1 induces apoptosis in the human myelogenous leukemia cell line THP-1 by a caspase-8-dependent, tumor necrosis factor receptor-independent mechanism. Infect. Immun. **73:**5115–5126.
31. **Lee, S.-Y., M.-S. Lee, R. P. Cherla, and V. L. Tesh.** 2008. Shiga toxin 1 induces apoptosis through the endoplasmic reticulum stress response in human monocytic cells. Cell Microbiol. **10:**770–780.
32. **Lingwood, C. A.** 1994. Verotoxin-binding in human renal sections. Nephron **66:**21–28.
33. **Lord, J. M., L. M. Roberts, and W. I. Lencer.** 2005. Entry of protein toxins into mammalian cells by crossing the endoplasmic reticulum membrane: co-opting basic mechanisms of endoplasmic reticulum-associated degradation. Curr. Top. Microbiol. Immunol. **300:**149–168.
34. **Murata, K., et al.** 2006. Verotoxin-1 stimulation of macrophage-like THP-1 cells up-regulates tissue factor expression through activation of c-Yes tyrosine kinase: possible signal transduction in tissue factor up-regulation. Biochim. Biophys. Acta **1762:**835–843.
35. **Nestoridi, E., R. I. Kushak, D. Duguerre, E. F. Grabowski, and J. R. Ingelfinger.** 2005. Up-regulation of tissue factor activity on human proximal tubular epithelial cells in response to Shiga toxin. Kidney Int. **67:**2254–2266.
36. **Obrig, T. G., T. P. Moran, and J. E. Brown.** 1987. The mode of action of Shiga toxin on peptide elongation of eukaryotic protein synthesis. Biochem. J. **244:**287–294.
37. **Orth, D., et al.** 2007. The Shiga toxin genotype rather than the amount of Shiga toxin or the cytotoxicity of Shiga toxin in vitro correlates with the appearance of the hemolytic uremic syndrome. Diagn. Microbiol. Infect. Dis. **59:**235–242.
38. **Proulx, F., E. G. Seidman, and D. Karpman.** 2001. Pathogenesis of Shiga toxin-associated hemolytic uremic syndrome. Pediatr. Res. **50:**163–171.
39. **Rao, R. V., H. M. Ellerby, and D. E. Bredesen.** 2004. Coupling endoplasmic reticulum stress to the cell death program. Cell Death Differ. **11:**372–380.
40. **Richardson, S. E., M. A. Karmali, L. E. Becker, and C. R. Smith.** 1988. The histopathology of the hemolytic uremic syndrome associated with verocytotoxin-producing *Escherichia coli* infections. Hum. Pathol. **19:**1102–1108.
41. **Rutkowski, D. T., and R. J. Kaufman.** 2004. A trip to the ER: coping with stress. Trends Cell Biol. **14:**20–28.
42. **Ryan, M. J., et al.** 1994. HK-2: an immortalized proximal tubule epithelial cell line from normal adult human kidney. Kidney Int. **45:**48–57.
43. **Sandvig, K.** 2001. Shiga toxins. Toxicon **39:**1629–1635.
44. **Sandvig, K., and B. van Deurs.** 2002. Transport of protein toxins into cells: pathways used by ricin, cholera toxin and Shiga toxin. FEBS Lett. **529:**49–53.
45. **Smith, W. E., et al.** 2003. Shiga toxin 1 triggers a ribotoxic stress response leading to p38 and JNK activation and induction of apoptosis in intestinal epithelial cells. Infect. Immun. **71:**1497–1504.
46. **Strockbine, N. A., M. P. Jackson, L. M. Sung, R. K. Holmes, and A. D. O'Brien.** 1988. Cloning and sequencing of the genes for Shiga toxin from *Shigella dysenteriae* type 1. J. Bacteriol. **170:**1116–1122.
47. **Strockbine, N. A., et al.** 1986. Two toxin-converting phages from *Escherichia coli* O157:H7 strain 933 encode antigenically distinct toxins with similar biologic activities. Infect. Immun. **53:**135–140.
48. **Takeda, T., et al.** 1993. Impairment by verotoxin of tubular function contributes to the renal damage seen in haemolytic uraemic syndrome. J. Infect. **27:**339–341.
49. **Tarr, P. I., C. A. Gordon, and W. L. Chandler.** 2005. Shiga-toxin-producing *Escherichia coli* and haemolytic uraemic syndrome. Lancet **365:**1073–1086.
50. **Tesh, V. L.** 2010. Induction of apoptosis by Shiga toxins. Future Microbiol. **5:**431–453.
51. **Tesh, V. L., et al.** 1993. Comparison of the relative toxicities of Shiga-like toxins type I and type II for mice. Infect. Immun. **61:**3392–3402.

52. **Tesh, V. L., J. E. Samuel, J. A. Burris, J. W. Owens, F. B. J. Taylor, Jr., and R. L. Siegler.** 1994. Quantitation and localization of shiga toxin/shiga-like toxin-binding glycolipid receptors in human and baboon tissues, p. 189–192. *In* M. A. Karmali and A. G. Goglio (ed.), Recent advances in verocytotoxin-producing *Escherichia coli* infections. Elsevier, Amsterdam, The Netherlands.
53. **Tewari, M., et al.** 1995. Yama/CPP32 beta, a mammalian homolog of CED-3, is a CrmA-inhibitable protease that cleaves the death substrate poly(ADP-ribose) polymerase. Cell **81:**801–809.
54. **Uchida, H., N. Kiyokawa, H. Horie, J. Fujimoto, and T. Takeda.** 1999. The detection of Shiga toxins in the kidney of a patient with hemolytic uremic syndrome. Pediatr. Res. **45:**133–137.
55. **Vittar, N. B., J. Awruch, K. Azizuddin, and V. Rivarola.** 2010. Caspase-independent apoptosis, in human MCF-7c3 breast cancer cells, following photodynamic therapy, with a novel water-soluble phthalocyanine. Int. J. Biochem. Cell Biol. **42:**1123–1131.
56. **Wilson, C., G. H. Foster, and M. Bitzan.** 2005. Silencing of Bak ameliorates apoptosis of human proximal tubular epithelial cells by *Escherichia coli*-derived Shiga toxin 2. Infection **33:**362–367.

Editor: S. M. Payne